Inorg. Chem. **2006**, *45*, 7224–7234

Zr^{IV}-Monosubstituted Keggin-Type Dimeric Polyoxometalates: Synthesis, Characterization, Catalysis of H_2O_2-Based Oxidations, and Theoretical Study

Oxana A. Kholdeeva,*,† Gennadii M. Maksimov,† Raisa I. Maksimovskaya,† Marina P. Vanina,† Tatiana A. Trubitsina,† Dmitry Yu. Naumov,‡ Boris A. Kolesov,‡ Nadya S. Antonova,§ Jorge J. Carbó,§ and Josep M. Poblet§

Boreskov Institute of Catalysis, Russian Academy of Sciences, Lavrentiev avenue 5, Novosibirsk 630090, Russia, Nikolaev Institute of Inorganic Chemistry, Russian Academy of Sciences, Lavrentiev avenue 3, Novosibirsk 630090, Russia, and Departament de Química Física i Inorgánica, Universitat Rovira i Virgili, Marcellí Domingo s/n, 43007 Tarragona, Spain

Received May 12, 2006

The previously unknown Zr^{IV}-monosubstituted Keggin-type polyoxometalates (Zr-POMs), $(n\text{-}Bu_4N)_7H[\{PW_{11}O_{39}Zr\text{-}(\mu\text{-}OH)\}_2]$ (**1**), $(n\text{-}Bu_4N)_8[\{PW_{11}O_{39}Zr(\mu\text{-}OH)\}_2]$ (**2**), and $(n\text{-}Bu_4N)_9[\{PW_{11}O_{39}Zr\}_2(\mu\text{-}OH)(\mu\text{-}O)]$ (**3**) differing in their protonation state, have been prepared starting from heteropolyacid $H_5PW_{11}ZrO_{40}\cdot 14H_2O$. The compounds were characterized by elemental analysis, potentiometric titration, X-ray single-crystal structure, and IR, Raman, and ^{31}P and ^{183}W NMR spectroscopy. The single-crystal X-ray analysis of **2** reveals that two Keggin structural units $[PW_{11}O_{39}Zr]^{3-}$ are linked through two hydroxo bridges Zr–(OH)–Zr with Zr^{IV} in 7-fold coordination. The IR spectra of **1** and **2** show a characteristic band at 772 cm^{-1}, which moves to 767 cm^{-1} for **3**, reflecting deprotonation of the Zr–(OH)–Zr bond. Potentiometric titration with methanolic Bu_4NOH indicates that **1**–**3** contain 2, 1, and 0 acid protons, respectively. ^{183}W NMR reveals C_s symmetry of **2** and **3** in dry MeCN, while for **1**, it discovers nonequivalence of its two subunits and their distortion resulting from localization of the acidic proton on one of the Zr–O–W bridging O atoms. The ^{31}P NMR spectra of **2** and **3** differ insignificantly in dry MeCN, showing only signals at δ –12.46 and –12.44 ppm, respectively, while the spectrum of **1** displays two resonances at δ –12.3 (narrow) and –13.2 (broad) ppm, indicating slow proton exchange on the ^{31}P NMR time scale. The theoretical calculations carried out at the density functional theory level on the dimeric species **1**–**3** propose that protonation at the Zr–O–Zr bridging site is more favorable than protonation at Zr–O–W sites. Calculations also revealed that the doubly bridged hydroxo structure is thermodynamically more stable than the singly bridged oxo structure, in marked contrast with analogous Ti- and Nb-monosubstituted polyoxometalates. The interaction of **1**–**3** with H_2O and H_2O_2 in MeCN has been studied by both ^{31}P and ^{183}W NMR. The stability of the $[PW_{11}O_{39}ZrOH]^{4-}$ structural unit toward at least 100-fold excess of H_2O_2 in MeCN was confirmed by both NMR and Raman spectroscopy. The interaction of **1** and **2** with H_2O in MeCN produces most likely monomeric species $(n\text{-}Bu_4N)_{3+n}[PW_{11}O_{39}Zr(OH)_n(H_2O)_{3-n}]$ ($n = 0$ and 1) showing a broad ^{31}P NMR signal at δ –13.2 ppm, while interaction with H_2O_2 leads to the formation of an unstable peroxo species (δ –12.3 ppm), which reacts rapidly with cyclohexene, producing 2-cyclohexen-1-one and *trans*-cyclohexane-1,2-diol. Both **1** and **2** show a pronounced catalytic activity in H_2O_2 decomposition and H_2O_2-based oxidation of organic substrates, including cyclohexene, α-pinene, and 2,3,6-trimethylphenol. The oxidation products are consistent with those of a homolytic oxidation mechanism. On the contrary, **3** containing no acid protons reacts with neither H_2O nor H_2O_2 and shows negligible catalytic activity. The Zr-monosubstituted polyoxometalates can be used as tractable homogeneous probes of Zr single-site heterogeneous catalysts in studying mechanisms of H_2O_2-based oxidations.

Introduction

Transition-metal-substituted polyoxometalates (POMs) are of scientific and industrial interest because of their varied and unique combination of properties, such as thermodynamic stability to oxidation, tunability of acid and redox

* To whom correspondence should be addressed. E-mail: khold@catalysis.nsk.su. Fax: (+7)383-330-95-73.

† Boreskov Institute of Catalysis, Russian Academy of Sciences.

‡ Nikolaev Institute of Inorganic Chemistry, Russian Academy of Sciences.

§ Universitat Rovira i Virgili.

10.1021/ic0608142 CCC: $33.50
Published on Web 08/09/2006

properties, solubility in various media, etc.[1−12] Because of the apparent structural analogies of POMs and metal oxide surfaces, these compounds can be viewed as discrete fragments of extended metal oxide lattices.[13−20] In the past decade, mechanistic studies based on soluble model catalytic systems are becoming increasingly important in the catalyst designing area.[21−30] The evident advantage of POMs as molecular probes that distinguishes them from organometallic compounds and complexes with organic ligands is thermodynamic stability of POMs toward oxidation and hydrolysis in a specific range of pH. Few research groups have applied POMs for probing mechanisms of heterogeneous catalysis.[15,31,32] Recently, Zr-containing polyoxotungstates were suggested as soluble analogues of heterogeneous tungstated zirconia catalysts.[33,34] We have gained a wide experience in using Ti-monosubstituted Keggin-type POMs for studying mechanisms of Ti-single-site-based catalysis.[35−41] In the present paper, we disseminate this approach with respect to Zr single-site catalysis. The growing number of applications of catalysts containing site-isolated Zr ions, including ZrS-1,[42] Zr-HMS,[43] Zr-MCM-41,[44−46] ZrO_2-SiO_2,[47,48] and Zr-MCF,[49] in selective oxidations with H_2O_2 has prompted us to prepare a Zr-monosubstituted Keggin-type POM (Zr-POM) and to study its ability to catalyze H_2O_2 oxidations. Note that several well-characterized Zr^{IV}-containing POMs have been known, including Zr-monosubstituted monomeric[33,34,50] and dimeric[33,51] polyoxotungstates of the Lindqvist structure, sandwich complexes $[Zr_3(\mu_2\text{-}OH)_3(A\text{-}\beta\text{-}SiW_9O_{34})2]^{11-}$,[52] $[Zr_4(\mu_3\text{-}O)_2(\mu_2\text{-}OH)_2(H_2O)_4(P_2W_{16}O_{59})_2]^{14-}$,[53] $[Zr_6O_2(OH)_4(H_2O)_3(\beta\text{-}SiW_{10}O_{37})_3]^{14-}$, and $[Zr_4O_2(OH)_2(H_2O)_4(\beta\text{-}SiW_{10}O_{37})_2]^{10-}$,[54] $[(\alpha\text{-}P_2W_{16}O_{59})Zr_2(\mu_3\text{-}O)(C_4O_5H_3)]_2^{18-}$,[55] and enantiomerically pure $\{[\alpha\text{-}P_2W_{15}O_{55}(H_2O)]Zr_3(\mu_3\text{-}O)(H_2O)(L\ (or\ D)\text{-}tartH)[\alpha\text{-}P_2W_{16}O_{59}]\}^{15-}$.[56]

(1) Pope, M. T. *Heteropoly and Isopoly Oxometalates*; Springer: Berlin, 1983.
(2) *Polyoxometalates: From Platonic Solids to Anti-Retroviral Activity*; Pope, M. T., Müller, A., Eds.; Kluwer: Dordrecht, The Netherlands, 1993.
(3) *Polyoxometalate Chemistry: From Topology via Self-Assembly to Applications*; Pope, M. T., Müller, A., Eds.; Kluwer: Dordrecht, The Netherlands, 2001.
(4) Moffat, J. B. *Metal−Oxygen Clusters: The Surface and Catalytic Properties of Heteropoly Oxometalates*; Kluwer/Plenum: New York, 2001.
(5) Kozhevnikov, I. V. *Catalysis by Polyoxometalates*; Wiley: Chichester, U.K., 2002.
(6) *Polyoxometalate Molecular Science*; Borrás-Almenar, J. J., Coronado, E., Müller, A., Pope, M. T., Eds.; Kluwer: Dordrecht, The Netherlands, 2003.
(7) *J. Mol. Catal*. **1996**, *114* (1−3), special issue on POMs.
(8) *Chem. Rev.* **1998**, *98*, special issue on POMs.
(9) Hill, C. L.; Prosser-McCartha, C. M. *Coord. Chem. Rev*. **1995**, *143*, 407−455.
(10) Neumann, R. *Prog. Inorg. Chem.* **1998**, *47*, 317−370 and references cited therein.
(11) Pope, M. T. Polyoxo Anions: Synthesis and Structure. In *Comprehensive Coordination Chemistry II*; Wedd, A. G., Ed.; Elsevier Science: New York, 2004; Vol. 4, pp 635−678.
(12) Hill, C. L. Polyoxometalates: Reactivity. In *Comprehensive Coordination Chemistry II*; Wedd, A. G., Ed.; Elsevier Science: New York, 2004; Vol. 4, pp 679−759.
(13) Baker, L. C. W. In *Advances in the Chemistry of Coordination Compounds*; Kirschner, S., Ed.; Macmillan: New York, 1961.
(14) Day, V. W.; Klemperer, W. G. *Science* **1985**, *228*, 533−541.
(15) Finke, R. G.; Rapko, B.; Saxton, R. J.; Domaille, P. J. *J. Am. Chem. Soc.* **1986**, *108*, 2947−2960 and references cited therein.
(16) Fournier, M.; Louis, C.; Che, M.; Chaquin, P.; Masure, D. *J. Catal*. **1989**, *119*, 400−414.
(17) Chen, Q.; Zubieta, J. *Coord. Chem. Rev.* **1992**, *114*, 107−167.
(18) Klemperer, W. G.; Marquart, T. A.; Yaghi, O. M. *Angew. Chem., Int. Ed.* **1992**, *31*, 49−51.
(19) Okuhara, T.; Mizuno, N.; Misono, N. *Adv. Catal*. **1996**, *41*, 113−252.
(20) Baker, L. C. W.; Glick, D. C. *Chem. Rev*. **1998**, *98*, 3−49.
(21) Feher, F. *J. Am. Chem. Soc*. **1986**, *108*, 3850−3852.
(22) Arzoumanian, H.; Baldi, A.; Lay, R.; Pierrot, M.; Petrignani, J. F.; Ridouane, F.; Sanchez. J.; Krentzien, H. In *The Role of Oxygen in Chemistry and Biochemistry, Studies in Organic Chemistry*; Ando, W., Moro-oka, Y., Eds.; Elsevier: Amsterdam, The Netherlands, 1988; Vol. 33, p 227.
(23) Basset, J.-M.; Candy, J.-P.; Choplin, A.; Didillon, B.; Quignard, F.; Theolier, A. In *Perspectives in Catalysis*; Thomas, J. M., Zamaraev, K. I., Eds.; Blackwell: Oxford, U.K., 1991; p 125.
(24) Edelmann, F. T. *Angew. Chem., Int. Ed. Engl.* **1992**, *31*, 586−587.
(25) Basset, J.-M.; Lefebvre, F.; Cantini, C. *Coord. Chem. Rev.* **1998**, *178*−*180*, 1703−1723.
(26) Lorenz, V.; Fischer, A.; Giessmann, S.; Gilje, J. W.; Gun'ko, Y.; Jacob, K.; Edelmann, F. T. *Coord. Chem. Rev.* **2000**, *206*−*207*, 321−368.
(27) Meunier, D.; Piechaczyk, A.; deMallmann, A.; Basset, J.-M. *Angew. Chem., Int. Ed.* **1999**, *38*, 3540−3542.
(28) Fandos, R.; Otero, A.; Rodriguez, A.; Ruiz, M. J.; Trreros, P. *Angew. Chem., Int. Ed.* **2001**, *40*, 2884−2886.
(29) Duchateau, R. *Chem. Rev*. **2002**, *102*, 3525−3542.
(30) Roesky, H. W.; Haiduc, I.; Hosmane, N. S. *Chem. Rev*. **2003**, *103*, 2579−2595.
(31) Mohs, T. R.; Du, Y. H.; Plashko, B.; Maatta, E. A. *Chem. Commun.* **1997**, 1707−1708.
(32) Ma, L.; Liu, S.; Zubieta, J. *Inorg. Chem.* **1989**, *28*, 175−177.
(33) Villanneau, R.; Carabineiro, H.; Carrier, X.; Thouvenot, R.; Herson, P.; Lemos, F.; Ribeiro, F. R.; Che, M. *J. Phys. Chem. B* **2004**, *108*, 12465−12471.
(34) Carabineiro, H.; Villanneau, R.; Carrier, X.; Herson, P.; Lemos, F.; Ribeiro, F.; Proust, A.; Che, M. *Inorg. Chem.* **2006**, *45*, 1915−1923.
(35) Kholdeeva, O. A.; Maksimov, G. M.; Maksimovskaya, R. I.; Kovaleva, L. A.; Fedotov, M. A. *React. Kinet. Catal. Lett.* **1999**, *66*, 311−317.
(36) Kholdeeva, O. A.; Maksimov, G. M.; Maksimovskaya, R. I.; Kovaleva, L. A.; Fedotov, M. A.; Grigoriev, V. A.; Hill, C. L. *Inorg. Chem.* **2000**, *39*, 3828−3837.
(37) Kholdeeva, O. A.; Kovaleva, L. A.; Maksimovskaya, R. I.; Maksimov, G. M. *J. Mol. Catal. A: Chem.* **2000**, *158*, 223−229.
(38) Kholdeeva, O. A.; Maksimovskaya, R. I.; Maksimov, G. M.; Kovaleva, L. A. *Kinet. Catal.* **2001**, *42*, 217−222.
(39) Kholdeeva, O. A.; Trubitsina, T. A.; Maksimovskaya, R. I.; Golovin, A. V.; Neiwert, W. A.; Kolesov, B. A.; López, X.; Poblet, J.-M. *Inorg. Chem.* **2004**, *43*, 2284−2292.
(40) Kholdeeva, O. A.; Trubitsina, T. A.; Maksimov, G. M.; Golovin, A. V.; Maksimovskaya, R. I. *Inorg. Chem.* **2005**, *44*, 1635−1642.
(41) Kholdeeva, O. A.; Trubitsina, T. A.; Timofeeva, M. N.; Maksimov, G. M.; Maksimovskaya, R. I.; Rogov, V. A. *J. Mol. Catal. A: Chem.* **2005**, *232*, 173−178.
(42) Dongare, M. K.; Singh, P.; Moghe, P. P.; Ratnasamy, P. *Zeolites* **1991**, *11*, 690−693.
(43) Besson, M.; Bonnet, M. C.; Gallezot, P.; Tkachenko, I.; Tuel, A. *Catal. Today* **1999**, *51*, 547−560.
(44) Chaudhari, K.; Bal, R.; Srinivas, D.; Chandwadkar, A. J.; Sivasanker, S. *Microporous Mesoporous Mater*. **2001**, *50*, 209−218.
(45) Zhu, Y.; Jaenicke, S.; Chuah, G. K. *J. Catal*. **2003**, *218*, 396−404.
(46) Wang, X.-X.; Veyre, L.; Lefebvre, F.; Patarin, J.; Basset, J.-M. *Microporous Mesoporous Mater*. **2003**, *66*, 169−179.
(47) Palazzi, C.; Oliva, L.; Signoretto, M.; Strukul, G. *J. Catal*. **2000**, *194*, 286−293.
(48) Morandin, M. J.; Gavagnin, R.; Pinna, F.; Strukul, G. *J. Catal*. **2002**, *212*, 193−200.
(49) Maksimchuk, N. V.; Melgunov, M. S.; Mrowiec-Białoń, J.; Jarzębski, A. B.; Kholdeeva, O. A. *J. Catal*. **2005**, *235*, 175−183.
(50) Chauveau, F.; Eberle, J.; Lefebvre, J. *Nouv. J. Chim*. **1985**, *9*, 315−320.
(51) Errington, R. J. In *Polyoxometalate Molecular Science*; Borrás-Almenar, J. J., Coronado, E., Müller, A., Pope, M. T., Eds.; Kluwer: Dordrecht, The Netherlands, 2003; p 55.
(52) Finke, R. G.; Rapko, B.; Weakley, T. J. R. *Inorg. Chem.* **1989**, *28*, 1573−1579.
(53) Gaunt, A. J.; May, I.; Collison, D.; Holman, K. T.; Pope, M. T. *J. Mol. Struct*. **2003**, *656*, 101−106.
(54) Bassil, B. S.; Dickman, M. H.; Kortz, U. *Inorg. Chem.* **2006**, *45*, 2394−2396.
(55) Fang, X.; Anderson, T.; Hill, C. *Chem. Commun*. **2005**, 5044−5046.

Herein we report the preparation and characterization of three Keggin-type Zr-POMs differing in their protonation state, $(n\text{-}Bu_4N)_7H[\{PW_{11}O_{39}Zr(\mu\text{-}OH)\}_2]$ (**1**), $(n\text{-}Bu_4N)_8[\{PW_{11}O_{39}Zr(\mu\text{-}OH)\}_2]$ (**2**), and $(n\text{-}Bu_4N)_9[\{PW_{11}O39Zr\}_2(\mu\text{-}OH)(\mu\text{-}O)]$ (**3**). The studies on the interaction of **1**−**3** with H_2O and H_2O_2 as well as their catalytic properties in H_2O_2-based oxidation of organic substrates are also reported. The question about crucial factors governing the catalytic activity of Zr centers is addressed.

Experimental Section

Materials. Acetonitrile (Fluka) was dried and stored over 4-Å molecular sieves. Tetra-*n*-butylammonium hydroxide, TBAOH (0.8 M solution in MeOH, Fluka), was titrated with 1.0 M HCl, while H_2O_2 (30 wt % in water) was titrated iodometrically prior to use. 2,3,6-Trimethylphenol (TMP) and cyclohexene (CyH) were purchased from Fluka. α-Pinene (98% α-pinene, 2% *β*-pinene) was obtained by vacuum rectification of gum turpentine. All of the other reactants were the best available reagent grade and were used without further purification.

Preparations. Heteropolyacid $H_5PW_{11}ZrO_{40}\cdot 14H_2O$ (Zr-HPA) was prepared by the electrodialysis method[57,58] analogously to $H_5PW_{11}TiO_{40}$, the synthesis of which had been recently described in detail.[40] To 30 mL of an aqueous solution (pH 6.3) of 0.3 M $Na_7[PW_{11}O_{39}]$ was added 2.9 g (9 mmol) of $ZrOCl_2\cdot 8H_2O$. This solution was filtered and exposed to electrodialysis for 5 h. The anolyte solution was steamed to dryness and then dried at 150 °C to remove residues of Cl_2. The resulting white solid was dissolved in 30 mL of water, filtered, and evaporated in a Petri dish to yield a straw-color glass. Yield: 27.5 g (99% based on W). Anal. Calcd for $H_{33}O_{54}PZrW_{11}$: P, 1.03; Zr, 2.99; W, 66.3. Found: P, 1.03; Zr, 2.95; W, 64.7. IR (1200−400, cm^{-1}): ν 1090, 1065, 970, 880, 785, 590, 505. ^{31}P NMR (in H_2O at 20 °C): δ −13.75. ^{31}P NMR in dry MeCN: δ −12.47. ^{183}W NMR (0.3 M in H_2O at 20 °C): δ −108.4(2), −109.1(1), −117.4(2), −128.3(2), −135.6(2), and −155.7(2). ^{17}O NMR (0.3 M in H_2O at 20 °C): δ 377, 401, 407, 521, 529, 710, 721, 731.

$(n\text{-}Bu_4N)_7H[\{PW_{11}O_{39}Zr(\mu\text{-}OH)\}_2]$ (1). To 25.15 g (8.2 mmol) of $H_5PW_{11}ZrO_{40}\cdot 14H_2O$ dissolved in 50 mL of water was added 41.2 mmol of tetrabutylammonium bromide (TBABr; 13.5 g dissolved in water). The resulting mixture was stirred thoroughly; then a white precipitate was separated by centrifugation, washed twice with 100 mL of H_2O, and dried at 150 °C. The resulting solid was dissolved in 100 mL of warm MeCN and reprecipitated by adding a 3-fold (v/v) excess of water, separated by filtration, washed with H_2O, and dried at 150 °C. Yield: 28.9 g (99%). Anal. Calcd for $C_{112}H_{253}N_7O_{80}P_2Zr_2W_{22}$ (fw 7269): C, 18.51; H, 3.54; N, 1.34; P, 0.85; Zr, 2.51; W, 55.6. Found: C, 16.61; H, 3.40; N, 1.32; P, 0.73; Zr, 2.38; W, 55.8. IR (KBr, 1100−500, cm^{-1}): ν 1063, 962, 890, 815, 772, 690, 595, 515. ^{31}P NMR (in dry MeCN at 20 °C): δ −12.36 (narrow) and −13.23 (broad). ^{31}P NMR [in MeCN/H_2O (20:1, v/v) at 20 °C]: δ −12.8. ^{183}W NMR [0.05 M in MeCN/H_2O (20:1, v/v) at 20 °C]: δ −98.9(2), −101.5(1), −108.0(2), −115.3(2), −117.3(2), and −143.0(2). Potentiometric titration of **1** (0.025 mmol) in MeCN (5 mL) with 0.8 M methanolic TBAOH, carried out as described in the literature,[15] showed a sharp breakpoint at 2 equiv of OH^-, indicating two acid protons in the molecule of **1**.

$(n\text{-}Bu_4N)_8[\{PW_{11}O_{39}Zr(\mu\text{-}OH)\}_2]$ (2). A total of 7.59 g (2.5 mmol) of $H_5PW_{11}ZrO_{40}\cdot 14H_2O$ was dissolved in 20 mL of H_2O. The solution was adjusted to pH 2.0 by adding solid $NaHCO_3$. After 2 h, 3.94 g (5 equiv) of TBABr dissolved in 20 mL of H_2O was added. The resulting mixture was vigorously stirred; then a white precipitate was separated by centrifugation, washed with 100 mL of H_2O, and dried at 150 °C. The resulting white solid was worked up as described for **1**. Yield: 9.21 g (99%). Anal. Calcd for $C_{128}H_{290}N_8O_{80}P_2Zr_2W_{22}$ (fw 7511): C, 20.47; H, 3.89; N, 1.49; P, 0.82; Zr, 2.43; W, 53.8. Found: C, 20.43; H, 3.99; N, 1.73; P, 0.88; Zr, 2.60; W, 54.0. IR (1100−500, cm^{-1}): ν 1062, 961, 889, 813, 772, 689, 595, 514. ^{31}P NMR (in dry MeCN at 20 °C): δ −12.46. ^{183}W NMR (0.05 M in dry MeCN at 20 °C): δ −94.5(2), −95.5(2), −98.9(1), −105.5(2), −118.1(2), and −122.4(2). Potentiometric titration with methanolic TBAOH revealed one acid proton in the molecule of **2**. To obtain crystals of **2**, 56 mg was dissolved in 3 mL of dry MeCN. Vapor diffusion of diethyl ether at room temperature for ca. 2 days resulted in the formation of X-ray-quality colorless prisms of **2**.

$(n\text{-}Bu_4N)_9[\{PW_{11}O_{39}Zr\}_2(\mu\text{-}OH)(\mu\text{-}O)]$ (3). To 20 mL of an aqueous solution of 0.3 M $Na_7[PW_{11}O_{39}]$ was added 1.94 g (6 mmol) of $ZrOCl_2\cdot 8H_2O$. The solution (pH 5.5) was filtered, and then 9.0 g (30 mmol) of TBABr dissolved in 30 mL of H_2O was added followed by a procedure described for **1**. Yield: 19.2 g (85%). Compound **3** was also prepared by adding 1 equiv of methanolic TBAOH to **2** dissolved in MeCN (or by adding 2 equiv of TBAOH to **1**) followed by precipitation of the solid by adding an excess of diethyl ether, filtration, and drying at 70 °C. Anal. Calcd for $C_{144}H_{325}N_9O_{80}P_2Zr_2W_{22}$ (fw 7752): C, 22.31; H, 4.23; N, 1.63; P, 0.80; Zr, 2.35; W, 52.2. Found: C, 20.18; H, 4.06; N, 1.44; P, 0.68; Zr, 2.45; W, 51.3. IR (1100−500, cm^{-1}): ν 1063, 960, 889, 814, 767, 685, 595, 514. ^{31}P NMR (in dry MeCN at 20 °C): δ −12.44. ^{183}W NMR (0.05 M in MeCN at 20 °C): δ −93.9(2), −94.9(2), −98.5(1), −104.9(2), −117.2(2), and −121.3(2). Potentiometric titration with methanolic TBAOH revealed no acid protons in the molecule of **3**.

Interaction of Zr-POMs with H_2O_2 and Catalytic Oxidations. Interaction of Zr-POMs with H_2O_2 was studied in MeCN at 20 °C using ^{31}P NMR ([Zr-POM] = 0.01 M and $[H_2O_2]$ = 0.02−2.0 M). H_2O_2 decomposition in the presence of Zr-POMs was studied in MeCN at 35 °C ([Zr-POM] = 0.0025−0.005 M and $[H_2O_2]$ = 0.16 M) by iodometric titration. Oxidation of CyH was studied at room temperature as follows. H_2O_2 (0.2 M) was added to a MeCN solution of Zr-POM (0.02 M), then 0.2 M CyH was added, and the reaction was followed by both ^{31}P NMR and gas chromatography (GC)−mass spectrometry (MS). Catalytic oxidations of TMP with H_2O_2 in the presence of Zr-POMs were carried out in temperature-controlled glass vessels at 80 °C, [Zr-POM] = 0.0025−0.005 M, [TMP] = 0.1 M, and $[H_2O_2]$ = 0.35 M. Biphenyl was added as the internal standard for GC. Catalytic oxidations of α-pinene were performed at 30 °C, [Zr-POM] = 0.0025 M, [α-pinene] = 0.1 M, and $[H_2O_2]$ = 0.12 M. Toluene was added as the internal standard. Samples were taken during the reaction course and analyzed by GC and GC−MS.

Instrumentation and Methods. Gas chromatographs Crystall-2000 and Tsvet-500 equipped with a flame ionization detector were used for GC analyses. Quartz capillary columns filled with Carbowax 20 M (25 m × 0.3 mm) and Supelco MDN-5S (30 m × 0.25 mm) were used for TMP and α-pinene oxidation products, respectively. GC−MS analyses were performed using a gas chromatograph Agilent 6890 (quartz capillary column 30 m × 0.25

(56) Fang, X.; Anderson, T.; Hill, C. L. *Angew. Chem., Int. Ed.* **2005**, *44*, 3540−3544.
(57) Kulikova, O. M.; Maksimovskaya, R. I.; Kulikov, S. M.; Kozhevnikov, I. V. *Izv. Akad. Nauk SSSR, Ser. Khim.* **1991**, *8*, 1726−1732.
(58) Maksimov, G. M.; Maksimovskaya, R. I.; Kozhevnikov, I. V. *Zh. Neorgan. Khim.* **1992**, *37*, 2279−2286.

mm/HP-5ms) equipped with a quadruple mass-selective detector Agilent MSD 5973. The ^{183}W NMR spectra were measured on MSL-400 and Avance-400 Bruker NMR spectrometers at an operating frequency of 16.67 MHz, with a 2.5-kHz sweep width, 50-μs pulse width, and 5-s pulse delay. The corresponding parameters for ^{31}P NMR were 161.98 MHz, 5 kHz, 10 μs, and 30 s. Chemical shifts, δ, were referenced to 85% H_3PO_4 and 2 M aqueous Na_2WO_4; for measuring ^{183}W δ values, a $H_4SiW_{12}O_{40}$ solution was used as a secondary standard (δ -103.65 ppm relative to WO_4^{2-}). The error in measuring δ was in the range of ± 0.05 and 0.1 ppm for ^{31}P and ^{183}W NMR spectra, respectively. The IR spectra were recorded for 0.5−1.0 wt % samples in KBr and in Nujol on Shimadzu FTIR-8300 and Scimitar FTS 2000 instruments. The Raman spectra were collected using a triple-grating spectrometer with a CCD detector. The 488-nm line of an Ar laser was used for the spectral excitation. The spectra were measured in 180° collection geometry with a Raman microscope. All measurements were performed with a spectral resolution of 5 cm^{-1}.

X-ray Crystallography and Data Collection. The crystals were removed from the glass in which they were grown together with a small amount of mother liquor and immediately coated with an epoxy resin on the microscope slide. A suitable crystal was mounted on the glass fiber with silicon grease and placed in the cold N_2 stream on an X8Apex Bruker-Nonius CCD with graphite-monochromated Mo Kα radiation at 250(2) K. After mounting, the temperature of the N_2 stream was decreased to 100(2) K by 50 K/h. No decay was observed in 18 duplicate frames at the end of data collection.

The structure was solved by direct methods, and the heavy atoms were located from an E map. The remaining non-H atoms were determined from successive difference Fourier syntheses. All non-H atoms were refined anisotropically using all data (based on F^2) with the software of *SHELXTL*.[59] An integration method using face indexes of the crystal was employed to correct for absorption.[60] H atoms were added geometrically and refined with a riding model.

Computational Details

The density functional theory (DFT) calculations discussed here were performed with the ADF 2004.01 package.[61] We applied the local density approximation featuring the Xα model with Becke's functional[62] for exchange and the VWN parametrization[63] with Perdew's correction[64] for correlation. The basis functions for describing the valence electrons of the atoms are Slater-type orbitals of triple-ζ + polarization quality. The internal or core electrons (O, 1s; P, 1s2s; Zr, 1s3d; W, 1s4d) were kept frozen. We applied scalar relativistic corrections to them—*zeroth-order regular approximation*—via the core potentials generated with the program DIRAC.[56] For the Lindqvist anions, the structures were optimized in the presence of the *conductor-like screening model* (COSMO),[65] implemented as a part of the ADF code. For the larger Keggin anions, the solvation energies were calculated, keeping the geometry optimized for the gas-phase species. To define the cavity surrounding the molecules, we used the solvent-excluding-surface method and fine tesserae. To obtain the electron density in solution, we first let the self-consistent field converge without solvent effects and, thereafter, turned on the COSMO to include the solvent effects variationally. The ionic radii for the POM atoms, which actually define the size of the solvent cavity where the target molecule remains, were chosen to be 0.74 Å for all metal ions. The radii for H and O are 1.20 and 1.52 Å, respectively. The dielectric constant (ϵ) utilized in the computations was set equal to 78 for modeling water (calculations on Lindqvist anions) and 36.6 for modeling the effects of acetonitrile (calculations on $PW_{11}ZrO_{40}^{5-}$ Keggin anions). When possible, optimizations under symmetry constraints were used in order to spare computational time. The constraints of the C_s symmetry group were used for the optimization of the structures **2**, **4**, and **2′c**, the C_{2v} symmetry group for the structures **2b**, **2′d**, and **3′**, and the D_{2h} symmetry group for the structures **2′** and **4′**.

Results and Discussion

Synthesis and Characterization of Dimeric Zr-POMs. The preparation of Zr-containing heteropolyacid $H_5PW_{11}ZrO_{40}\cdot nH_2O$ was first described in 1992.[58] On the basis of the results of elemental analysis, IR, and ^{31}P and ^{183}W NMR, the above-mentioned formula was ascribed. However, keeping in mind that coordination numbers typical of Zr^{IV} complexes, including POMs,[33,34,51−56] are 7 and 8, we cannot exclude that in the solid state Zr-HPA may have a dimeric structure similar to that of **2** (vide infra). On the basis of the analogy with the Lindqvist-type polyanion $[W_5O_{18}\{Zr(H_2O)_3\}]^{2-}$ recently described by Villanneau et al.,[34] a monomeric structure $H_3[PW_{11}O_{39}\{Zr(H_2O)_n\}]$ ($n = 2$ and 3) also cannot be ruled out in aqueous solution.

The interaction of Zr-HPA with a 5-fold excess of TBABr in aqueous solution at different pH values (see the Experimental Section) resulted in the formation of TBA salts of the Keggin-type Zr-POM, **1** and **2**. In turn, **2** can be easily obtained from **1** by adding 1 equiv of TBAOH, while adding 2 and 1 equiv of TBAOH to **1** and **2**, respectively, yields compound **3**. An alternative procedure involving the interaction of $Na_7[PW_{11}O_{39}]$ and $ZrOCl_2\cdot 8H_2O$ followed by precipitation with TBABr at pH 5.5 leads to **3**. The different composition of the cationic part of **1**−**3** was unambiguously indicated by both C, H, and N elemental analyses and potentiometric titration with methanolic TBAOH in MeCN. Additionally, the different protonation state in Zr-POMs was inferred from a combination of spectroscopic techniques (vide infra).

(59) Bruker AXS Inc. *SHELXTL*, version 6.12; Bruker Advanced X-ray Solutions: Madison, WI, 2004.
(60) Bruker AXS Inc. *SADABS*, version 2.11; Bruker Advanced X-ray Solutions: Madison, WI, 2004.
(61) ADF 2004.01, Department of Theoretical Chemistry, Vrije Universiteit, Amsterdam, The Netherlands, 2004. Baerends, E. J.; Ellis, D. E.; Ros, P. *Chem. Phys.* **1973**, *2*, 41. Versluis, L.; Ziegler, T. *J. Chem. Phys.* **1988**, *88*, 322. Te Velde, G.; Baerends, E. J. *J. Comput. Phys.* **1992**, *99*, 84. Fonseca Guerra, C.; Snijders, J. G.; Te Velde, G.; Baerends, E. J. *Theor. Chem. Acc.* **1998**, *99*, 391.
(62) Becke, A. D. *J. Chem. Phys.* **1986**, *84*, 4524. Becke, A. D. *Phys. Rev.* **1988**, *A38*, 3098.
(63) Vosko, S. H.; Wilk, L.; Nusair, M. *Can. J. Phys.* **1980**, *58*, 1200.
(64) Perdew, J. P. *Phys. Rev.* **1986**, *B33*, 8822. Perdew, J. P. *Phys. Rev.* **1986**, *B34*, 7406.
(65) Klamt, A.; Schüürmann, G. *J. Chem. Soc., Perkin Trans. 2* **1993**, 799. Andzelm, J.; Kölmel, C.; Klamt, A. *J. Chem. Phys.* **1995**, *103*, 9312. Klamt, A. *J. Chem. Phys.* **1995**, *99*, 2224. Model implemented in the ADF package by Pye, C. C.; Ziegler, T. *Theor. Chem. Acc.* **1999**, *101*, 396.

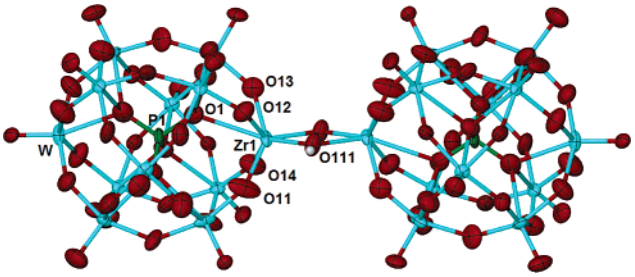

Figure 1. Molecular representation of the POM anion of compound **2**.

Table 1. Crystal Data and Data Collection Parameters for **2**

formula	$C_{128}H_{290}N_8O_{80}P_2W_{22}Zr_2$
fw	7510.76
T, K	100(2)
λ, Å	0.710 73
cryst syst	monoclinic
space group	$P2_1/n$
a, Å	15.104(2)
b, Å	47.406(7)
c, Å	15.344(2)
α, deg	90
β, deg	109.130(2)
γ, deg	90
V, Å^3	10380(2)
Z	2
ρ, g/cm^3	2.403
μ, mm^{-1}	12.319
cryst size, mm^3	0.22 × 0.25 × 0.13
R1 (obsd data)	0.0690
wR2 (all data)	0.1309

Table 2. Selected Bond Lengths [Å] for **2**

Zr1−O11	2.031(16)	Zr1−O111	2.061(14)
Zr1−O12	2.080(14)	Zr1−O111′	2.127(14)
Zr1−O13	2.062(14)	Zr1−O1	2.708(15)
Zr1−O14	2.089(15)		

A slow vapor diffusion of diethyl ether to dilute MeCN solutions of **2** at room temperature yielded X-ray-quality colorless prisms having similar crystallographic parameters consistent with the crystal structure shown in Figure 1. The corresponding crystal data and selected bond distances are given in Tables 1 and 2, respectively. The single-crystal X-ray analysis of **2** revealed that two $[PW_{11}O_{39}Zr]^{3-}$ structural subunits are linked through two hydroxo bridges Zr−(OH)−Zr. In dimeric anion **2**, Zr^{IV} is seven-coordinated to five O atoms of the lacunary Keggin unit and two *μ*-OH ligands. Note that seven-coordinated hydroxo-bridged Zr^{IV} complexes are well-precedented. A similar structure has been recently reported for the Lindqvist-type Zr-substituted polyoxotungstate $(Bu_4N)_6[\{W_5O_{18}Zr(\mu\text{-}OH)\}_2]\cdot 2H_2O$.[33,34] Packing diagrams of compound **2** viewed down the *a* and *c* axes are shown in Figure S1 in the Supporting Information (SI). X-ray analysis revealed the presence of eight TBA cations per one anion of **2**. Evidence for the composition of **2** was also provided by the elemental analysis for C, H, N, P, Zr, and W (and Na = 0) and thermal gravimetric analysis (TGA), which showed no detectable (<0.5%) weight loss below 200 °C indicative of the absence (<$2H_2O$) of any lattice water.

Potentiometric titration of **1** and **2** in MeCN with methanolic TBAOH showed a sharp breakpoint upon the addition of 2 and 1 equiv of TBAOH (Figure S2 in the SI), thus indicating the presence of two and one acid protons in the molecules of **1** and **2**, respectively. However, keeping in mind the C, H, and N elemental analyses data, which are more consistent with seven and eight TBA cations in **1** and **2** rather than with eight and nine, one can calculate that three and two protons are required to fulfill the charge balance of **1** and **2**, respectively. In turn, potentiometric titration of **3** revealed no acid protons, while the elemental analyses supported the composition with 9 rather than 10 TBA cations. Importantly, no Na (<0.001%) was found in **1**−**3**. This means that the third proton in Zr-POM is strongly bound to the Zr−O−Zr bridging O atom (does not possess acidic properties) and thus cannot be determined by the potentiometric titration.

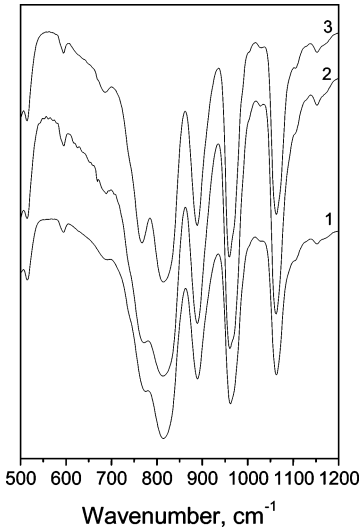

Figure 2. IR spectra (500−1200 cm^{-1}) of Zr-POMs (1%) in KBr: $(n\text{-}Bu_4N)_7H[\{PW_{11}O_{39}Zr(\mu\text{-}OH)\}_2]$ (**1**), $(n\text{-}Bu_4N)_8[\{PW_{11}O_{39}Zr(\mu\text{-}OH)\}_2]$ (**2**), and $(n\text{-}Bu_4N)_9[\{PW_{11}O_{39}Zr\}_2(\mu\text{-}OH)(\mu\text{-}O)]$ (**3**).

The IR spectra of solid **1**−**3** are very similar and display a fingerprint region that is characteristic of Keggin-type POMs (Figure 2). The spectra of **1** and **2** show a characteristic band located at 772 cm^{-1}, which moves to 767 cm^{-1} in the spectrum of **3**. Apparently, the intensity of this band increases upon deprotonation. Note that a general decrease in energy for POM vibrations upon deprotonation has been already documented.[15] Previously, we found that the Keggin *μ*-oxo and *μ*-hydroxo Ti-POM dimers also have a small difference in the positions of the Ti−O−Ti and Ti−(OH)−Ti bands, which are located at 640 and 655 cm^{-1},[36,40] respectively. Therefore, we may assume that the IR feature at 767 cm^{-1} is a manifestation of Zr−O−Zr bonds. Interestingly, the IR spectrum of dimeric polyoxotungstate $(Bu_4N)_6[\{W_5O_{18}Zr(\mu\text{-}OH)\}_2]$ shows an intense band located at 730 cm^{-1}, while the corresponding monomeric species does not.[33] The presence of a 785-cm^{-1} feature in the IR spectrum of Zr-HPA (see the Experimental Section) allows the suggestion of a dimeric structure in the solid state. The IR spectra of **1**−**3** collected in Nujol differ in their 1600−1800- and 3000−4000-cm^{-1} localities (Figure S3 in the SI). No bands in the range of 1600−1800 cm^{-1} were found for **3**, while the spectra of **1** and **2** showed a characteristic feature at about 1620 cm^{-1}, which according to the literature should be attributed to H_2O.[15,66] Because neither X-ray analysis nor TGA (detection limit is $2H_2O$) indicated any lattice water,

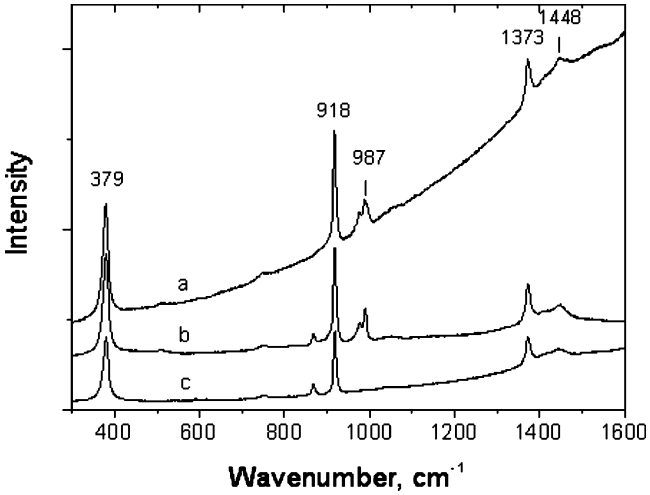

Figure 3. Raman spectra in MeCN: **1**, 0.01 M (a), **1** after the addition of a 100-fold excess of H_2O_2 (b), and H_2O_2, 1 M (c).

we believe that some small amount of H_2O may be due to its adsorption during collection of the spectra. Significantly, no characteristic vibration around 1715 cm^{-1} was manifested in the IR spectra of **1**−**3**, which implies that no H_3O^+ was present in Zr-POMs.[15,66] The IR spectra of both **1** and **2** show high-frequency ν_{OH} bands at about 3640 (sharp) and 3500 (broad) cm^{-1}, which can be assigned to OH ligands, isolated, and H-bonded, respectively.[67] The spectrum of **3** shows only a weak sharp band at 3655 cm^{-1}.

The Raman spectra of solid **1**−**3** are very similar (Figure S4 in the SI) and resemble the spectra of other Keggin-type POMs, specifically, Ti-POM.[39] Some broadening of the Raman bands can be seen in the spectrum of **1**. Importantly, the Raman spectra of solid **1**−**3** and their solutions in MeCN (compare Figures 3a and S4 in the SI) are quite similar, indicating the retention of the structure in solution.

The ^{31}P NMR spectra of **2** and **3** differ insignificantly in dry MeCN, both showing singlets at δ −12.46 and −12.44 ppm, respectively (Figure 4a, B and C), which corresponds to the equivalence of the halves of these dimers, while dimer **1** shows two ^{31}P NMR signals of comparable intensity: at δ −12.3 (narrow, ∼3 Hz) and −13.2 (broad, up to 50 Hz) ppm (Figures 4Aa and S5a in the SI). This suggests that the third proton is localized on the Zr−O−W bridge of one of the subunits, shifting and broadening the ^{31}P NMR signal owing to the dipole−dipole interaction of the P atom with a firmly attached proton, as was observed by Finke et al.[15] for the ^{29}Si NMR signal of $TBA_4H_3SiW_9V_3O_{40}$ in dry MeCN. This hypothesis is strongly supported by the fact that both the chemical shift and the signal width are very sensitive to the amount of water in MeCN (Figure S5a−d in the SI). Keeping in mind the previous H^+ mobility studies,[15,68] we anticipated that adding water or base to a MeCN solution of **1** would increase the mobility of the protons and accelerate the mutual site exchange process, resulting in the narrowing of the signal of the protonated subunit and its averaging with

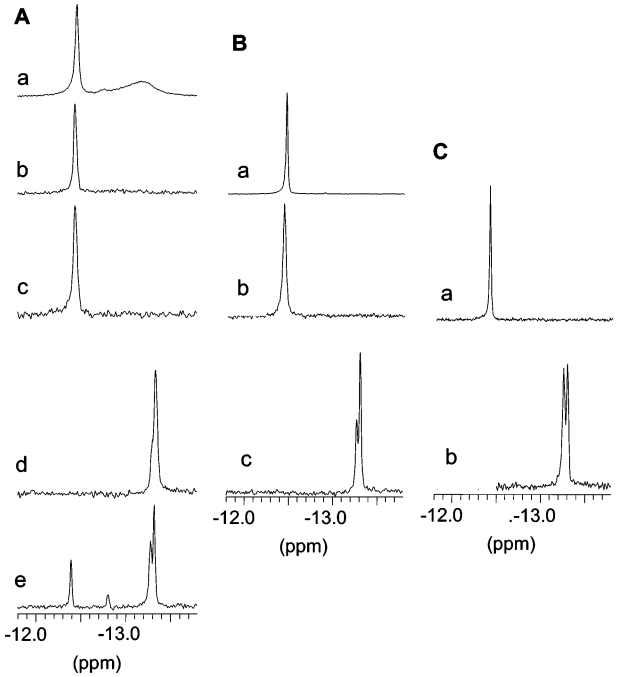

Figure 4. ^{31}P NMR spectra of Zr-POMs upon the addition of TBAOH ([Zr-POM] = 0.005 M, MeCN, 20 °C). A: **1** (a), **1** immediately after the addition of 1.0 (b), 2.0 (c), and 4.0 and 5.0 (d) equiv of TBAOH, and **1** + 5.0 equiv of TBAOH in 5 days (e). B: **2** (a), **2** after the addition of 1.0 (b) and 2.0 (c) equiv of TBAOH. C: **3** (a) and **3** + 1.4 equiv of TBAOH in 2 days (b).

the signal of the other half. Indeed, that was exactly what happened upon the addition of a certain amount (2% v/v) of water (Figure S5d in the SI) or small amounts (0.25 equiv) of TBAOH. Additionally, the broad signal disappeared upon storage of the solution over activated 3-Å molecular sieves.

The conclusions about the structure and composition of **1**−**3** and about slow proton exchange in **1** based on ^{31}P NMR and other techniques are strongly supported by the ^{183}W NMR data, which are presented in Figure 5. Unfortunately, the low solubility of TBA salts of Zr-POMs does not allow us to get spectra with a better signal-to-noise ratio. However, six lines with an intensity ratio approximately equal to 2:2:1:2:2:2 are clearly seen and provide evidence for the C_s symmetry of **2** and **3**. In dry MeCN, **1** gives nine broadened signals with the approximate intensity ratio 4:2:4:2:(4 + 2):2:1:1 (Figure 5f) instead of six signals observed for **2** and **3**. Upon the addition of H_2O, the three more broadened and upfield-shifted signals coalesce into one broad peak, which tends to the W4 resonance in the spectra of **2** and **3**, while the two other signals of the intensity 2 also coalesce into one signal, corresponding to atom W1 (W1 and W4 are linked with Zr by bent (1) and quasi-linear (4) W−O−Zr bridges, respectively). The observed splitting, shifting, and broadening of the signals indicate that the proton is localized on one of the four W4−O−Zr bridges of dimer **1**. The resulting distortion of the structure causes splitting of the peaks, which is more pronounced for the nearest W atoms. For the more distant W atoms, the splitting manifests as the noticeable signal broadening. Again, small additives of water (or aqueous H_2O_2) promote the site exchange process (slow-intermediate on the NMR time scale) and bring the compli-

(66) Highfield, J. G.; Moffat, J. B. *J. Catal.* **1984**, *88*, 177−187.
(67) Jeffrey, G. A. *An introduction to hydrogen bonding*; Oxford University Press: New York, 1997; p 303.
(68) Harmalker, S. P.; Pope, M. T. *J. Inorg. Biochem.* **1986**, *28*, 85−95.

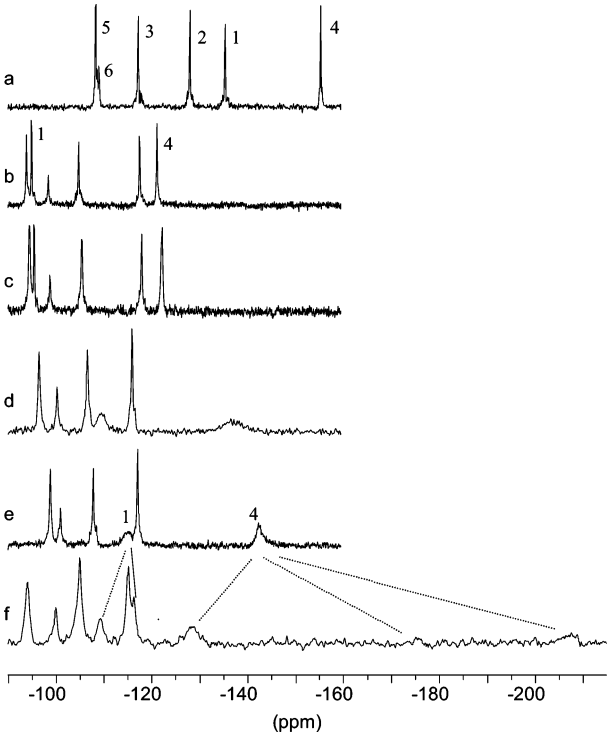

Figure 5. ^{183}W NMR spectra of Zr-POMs: $H_5PW_{11}ZrO_{40}$ (a), **3** (b), **2** (c), **1** in MeCN/H_2O (20:1, v/v) (d), **1** after the addition of a 2-fold molar excess of H_2O_2 (e), and **1** (f). The spectra of **1**−**3** (0.05 M) were run at 20 °C (b, c, and f, in dry MeCN). The spectrum of Zr-HPA (0.3 M) was collected in water at 20 °C.

cated spectrum closer to the six-line pattern typical of the C_s symmetry (Figure 5d,e).

DFT Studies on Dimeric Species. The experimentally prepared Zr-monosubstituted dimeric POMs have been investigated by means of DFT calculations. Initially, we optimized the structures of $H[\{PW_{11}O_{39}Zr(\mu\text{-}OH)\}_2]^{7-}$ (**1**), $[\{PW_{11}O_{39}Zr(\mu\text{-}OH)\}_2]^{8-}$ (**2**), and $[\{PW_{11}O_{39}Zr\}_2(\mu\text{-}OH)(\mu\text{-}O)]^{9-}$ (**3**) POMs. In the case of **1**, the protons are located at the Zr−O−Zr and Zr−O−W bridging O atoms. The three structures are computationally characterized as stationary points at the potential energy surface. The computed geometry for **2** is in general good agreement with that experimentally determined by X-ray. However, the distances between the Zr atoms and the Zr−O−Zr bridging O atoms are computed to be slightly longer than the experimental ones (0.11 Å on average). We have already assessed that the optimization of the structures including solvation improves the geometries.[69] To determine the effects of solvent on geometries, the relatively small Lindqvist analogues are used here as a model for the analysis of large Keggin structures, whose size is at the limit of our computational resources. In the computed gas-phase geometry of $[\{W_5O_{18}Zr(\mu\text{-}OH)\}_2]^{6-}$ (**2′**), the Zr−O(H) distances are 0.07 Å longer than the average distances in the corresponding X-ray structure.[33] The optimization in the presence of a model solvent (see the Computational Details section) ended in a structure, in which the Zr−O(H) distances are only 0.02 Å longer than the experimentally observed distances. It seems that the solvent effect minimizes the repulsion between the two highly charged subunits, allowing them to stay closer and reach values in better agreement the experimental ones. Nevertheless, as we will discuss below, these geometrical differences do not have a significant influence on the energy of Zr linkages. The removal of one proton of species **2** to form **3** causes a significant shortening of the Zr−(μ-O)−Zr bond distances by about 0.2 Å at our level of theory. Accordingly, the distance between the two Keggin cluster anions decreases by about 0.27 Å. Analogously, the addition of one proton to the bridging W−O−Zr O atom to form **1** produces a lengthening of the involved M−O bonds (by 0.18 and 0.26 Å for Zr−O and W−O bonds, respectively). The geometrical parameters related to the two hydroxo bridges do not vary significantly.

Additionally, we also evaluated other possible isomers of the X-ray-determined structure **2** of C_s symmetry. First, the variation of the relative disposition of the two Keggin-type $[PW_{11}O_{39}Zr]$ subunits could form a new structure **2b** of C_{2v} symmetry. In **2b**, only one W atom of each subunit lies in the plane formed by the Zr atoms and the μ-hydroxo ligands, whereas in **2**, three W atoms of each subunit were roughly in that plane (see the SI for details). We did not observe significant changes in bond lengths or bond angles on going from **2** to **2b**. This latter isomer is only 2.2 kcal/mol less stable than **2**, suggesting that both isomers could coexist, depending on the experimental conditions. Second, NMR data suggest that proton-exchange processes between W−O−Zr bridges, which are accelerated by the addition of water or base, occur in structure **1**. Thus, it is reasonable to think that other isomers could be formed by migration of one proton from the Zr−O−Zr bridging O atom in **2**. To assess this and to evaluate the feasibility of proton exchange between Zr−O−Zr and W−O−Zr bridging sites, we optimized the model Lindqvist dimeric structures $H[\{W_5O_{18}Zr\}_2(\mu\text{-}OH)(\mu\text{-}O)]^{6-}$ (**2′c**) and $H_2[\{W_5O_{18}Zr\}_2(\mu\text{-}O)_2]^{6-}$ (**2′d**). Because Keggin and Lindqvist Zr dimers exhibit a qualitatively similar experimental[33] and computational behavior (see below), hereinafter we will use Lindqvist structures as more affordable models of Keggin POMs, aiming to perform more detailed studies on these dimers. The relative energies of **2′**, **2′c**, and **2′d** are 0.0, +15.1, and +30.8 kcal/mol, respectively. This indicates that the preferred site for protonation is Zr−O−Zr, in agreement with the experimental results and our previous computational findings.[65] We have recently shown that the substitution of W^{VI} by a metal with lower oxidation state such as V^V, Nb^V, or Ti^{IV} increases the overall basicity of POM and, in particular, the nucleophilicity of the substituted region.[70] Moreover, the protonation energy difference between the two bridging O sites is relatively large (15 kcal/mol), which does not support a rapid proton-exchange process in **2**.

Notably, the dimerization products of Zr-monosubstituted Keggin and Lindqvist[33] anions show a marked contrast with

(69) López, X.; Fernández, J. A.; Romo, S.; Paul, J. F.; Kazansky, J. M.; Poblet, J. M. *J. Comput. Chem.* **2004**, *25*, 1541. Poblet, J. M.; López, X.; Bo, C. *Chem. Soc. Rev.* **2003**, *32*, 297.

(70) López, X.; Bo, C.; Poblet, J. M. *J. Am. Chem. Soc.* **2002**, *124*, 12574−12582. Fernández, J. A.; López, X.; Poblet, J. M. *J. Mol. Catal. A* **2006**, in press.

Scheme 1

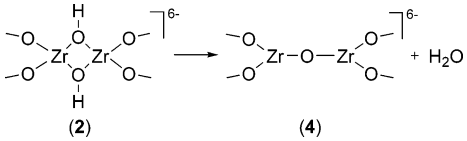

(**2**) (**4**)

other analogous early-transition-metal-monosubstituted POMs. In the Zr case, two μ-hydroxo ligands link the metals, whereas for Nb[71] and Ti,[36,40] the intercluster linkages contain only one M−(μ-OH)−M or M−(μ-O)−M junction (M = Nb or Ti). The proposed mechanism for dimerization of Ti^{IV}-monosubstituted Keggin-type POMs[36] consists of a condensation of two protonated monomers to yield the monobridged dimer and a water molecule. This mechanism might probably involve a doubly bridged intermediate equivalent to species **2**. In fact, the characterization of **2** for the Zr case is, in turn, an indication for the existence of that intermediate for the Ti and Nb cases. It seems that, depending on the nature of the substitution, the dimerization process stops at the doubly bridged intermediate or evolves to a singly bridged dimer. We computed the energy cost for the loss of a water molecule in **2′** to give the mono-oxo-bridged dimer $[\{W_5O_{18}Zr\}_2(\mu\text{-O})]^{6-}$ (**4′**; Scheme 1). The process is endothermic by 3.1 kcal/mol. For the analogous Lindquist structures, the reaction **2** → $[\{PW_{11}O_{39}Zr\}_2(\mu\text{-O})]^{8-}$ (**4**) + H_2O is also endothermic by 9.5 kcal/mol, supporting the extrapolation of the results obtained with Lindqvist structures. On the contrary, we have previously found that the formation of $[\{W_5O_{18}M\}_2(\mu\text{-O})]^{6-}$ from $[\{W_5O_{18}M(\mu\text{-OH})\}_2]^{6-}$ (M = Nb or Ti) is exothermic by 2.0 and 14.7 kcal/mol, respectively.[72,72] These results are indicative of a thermodynamic preference for a doubly bridged hydroxo dimer in Zr-monosubstituted Keggin and Lindqvist dimers, whereas for the analogous Ti and Nb species, the experimentally obtained mono-oxo dimer is preferred. We also checked the thermodynamic stability toward water loss of the triprotonated structure **1**. As for diprotonated species, the calculated energy for the reaction of $H[\{W_5O_{18}Zr(\mu\text{-OH})\}_2]^{5-}$ (**1′**) to give $H[\{W_5O_{18}Zr\}_2(\mu\text{-O})]^{5-}$ (**5′**) and water is endothermic (about +1.1 kcal/mol), further supporting the stability of triprotonated species. This small energy difference is within the limits of accuracy of the modeling and the methodology employed. However, the value is qualitatively very similar to that computed for mono-oxo-bridged dimer formation from **2′**, and it is fully consistent with the experimental findings. For **3**, the mechanism of water loss would probably imply a previous protonation to yield **1** or **2**, and therefore the process could also be precluded.

Finally, we examined the monomerization process for species **2′**, **2′c**, and **2′d** (Scheme 2). The quantitative assessment of these processes involving charge separation is not an easy task because it requires an accurate accounting of the solvent effects for the differently charged species. However, valuable information can be obtained in the

Scheme 2

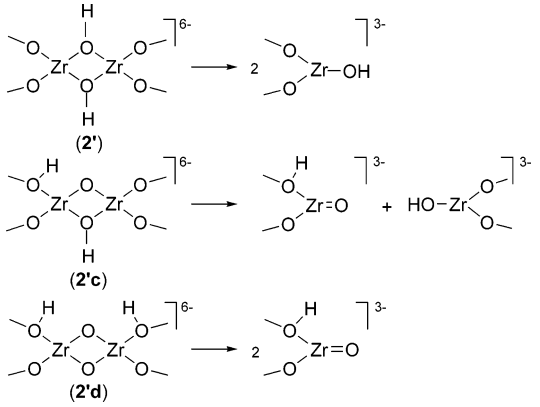

comparison of the three processes, for which the same charge separation occurs. This series of processes involves the breaking of two Zr−OH, one Zr−OH and one Zr−O, and two Zr−O bonds for **2′**, **2′c**, and **2′d**, respectively (Scheme 2). Thus, the comparison of their energy costs can be used to roughly evaluate the difference between hydroxo and oxo bond strengths. All monomerizations are endothermic by 5.8, 7.3, and 8.2 kcal/mol for **2′**, **2′c**, and **2′d**, respectively, with the breaking of two Zr−O bonds being the highest energy process. More interestingly, on going from **2′** to **2′c** and from **2′c** to **2′d**, the energy cost increases only by about 1−2 kcal/mol, which can be assigned to the variation between bond strengths. Thus, our calculations predict that the Zr−O bond is only slightly stronger than the Zr−OH bond. Obviously, this amount of energy could be largely compensated for by protonation energies at those oxo sites. Moreover, the Zr doubly bridged dimers not only are more thermodynamically stable than the corresponding singly bridged ones but also show a thermodynamic preference for the dimeric forms over the monomeric ones. We have commented above that inclusion of the solvent effect caused a significant variation in the bond lengths for the Zr−μ-OH−Zr bridges in **2′** species. However, the monomerization energy computed at the gas-phase geometry does not vary dramatically (7.8 and 5.8 kcal/mol at the gas phase and in the presence of the model solvent, respectively). This result suggests that the Zr−O bonds bridging the two POM subunits are relatively flexible.

Interaction of Zr-POMs with H_2O and TBAOH. A significant upfield shift accompanied by broadening of the ^{31}P NMR signal upon further (>2% v/v) addition of water to the MeCN solution of **1** (Figure S5e−g in the SI) cannot be attributed only to the change of the solution magnetic susceptibility. A similar signal shift and broadening was also found for **2**. On the contrary, the spectrum of **3** was not sensitive to the presence of H_2O in MeCN. In contrast to Ti-POMs,[39−41] we cannot ascribe the observed (upfield) shift of the ^{31}P NMR resonance to deprotonation of **2** upon the addition of water because transformation of **2** to **3** upon the addition of 1 equiv of TBAOH caused no change in the signal position (Figure 4Bb). This implies that some other process occurs with **1** and **2** in the presence of water. We suppose that a monomerization process most likely takes place when **1** and **2** are allowed to react with H_2O. The process is evidently assisted by acid protons present in **1**

(71) Clegg, W.; Elsegood, M. R. J.; Errington, J.; Havelock, J. *J. Chem. Soc., Dalton Trans.* **1996**, 681.
(72) López, X.; Weinstock, I. A.; Bo, C.; Sarasa, J. P.; Poblet, J. M. Submitted for publication.

and **2**. Keeping in mind that Zr^{IV} is typically seven-coordinated or more often eight-coordinated, we anticipated that this interaction would produce monomeric species $(n\text{-}Bu_4N)_{3+n}[PW_{11}O_{39}Zr(OH)_n(H_2O)_{3(2)-n}]$ ($n = 0$ and 1), which display a broad ^{31}P NMR signal at about δ −13.2 ppm. The signal broadening may be due to exchange between species containing different amounts of coordination water. Our attempts to isolate such monomeric species failed because of their tendency to dimerize during the crystallization process.

As we mentioned already, the addition of 1 equiv of base to **2** produces no changes in either the position or width of the ^{31}P NMR signal. Hence, no degradation of the dimeric structure occurs upon deprotonation of one of the Zr−O(H)−Zr bridging O atoms. However, further addition of TBAOH to **3** (or to preliminarily neutralized **1** and **2**) causes upfield shifting of the ^{31}P NMR signal and its splitting into two signals at δ −13.27 and −13.31 ppm (Figure 4A−C), the ratio between which depends on the amount of TBAOH added. Interestingly, the intensity of the signal with δ −13.27 ppm slightly increased after allowing the solutions to stand for a few days. When 5 equiv of TBAOH was added to **1**, the ^{31}P NMR spectrum drastically changed in several days and displayed again the signal at δ −12.47 ppm, a new unidentified signal at δ −12.80 ppm, and signals at δ −13.27 and −13.31 ppm (Figure 4Ae). A similar process was observed while adding alkali ($NaHCO_3$) to an aqueous solution of Zr-HPA. The chemical shift of the ^{31}P NMR resonance of Zr-HPA remained unchanged (δ −13.77 ppm) up to pH 3.2, but a further increase in the pH resulted in the gradual appearance of two new signals at δ −14.70 and −14.81 ppm with an approximately 1:1 intensity ratio. After the pH reached 6.1, the signal at δ −13.77 ppm completely disappeared. We might suggest that unstable monomeric and/or dimeric Zr-POM species (probably those having terminal Zr−OH and/or Zr═O bonds) form initially upon the addition of OH^- to **3** followed by slow partial escape of Zr from the Keggin structure to produce a 1:2 anion $[Zr(PW_{11}O_{39})_2]^{10-}$ and slow partial redimerization of the monomeric species to produce **3**. It is worth noting that increasing the solution basicity, which results in upfield shifting and splitting of the ^{31}P NMR signal, also leads to the transformation of the six-line ^{183}W NMR spectrum to a more complicated one showing 20 signals (two signals are superposition of four) and thus reflecting a disturbance of the C_s symmetry. In fact, the 22-line spectrum may indicate the presence of two Zr-POMs having C_i symmetry. Such POMs might be produced by alkaline hydrolysis of Zr−O−Zr bridges in the molecule of **3**, leading to the formation of heteropolyanions with external Zr−OH and Zr═O bonds, e.g., $[PW_{11}O_{39}Zr(O)_n(OH)_{3-n}]^{m-}$ ($n = 1$ and 2). Previously, we found that Ti-POMs with terminal Ti═O and Ti−OH bonds do not exchange on the NMR time scale in MeCN and thus show two close but distinguishable ^{31}P NMR resonances.[36,40] Further spectroscopic studies, which are in progress in our groups, should gain insight into the interconversion chemistry of different Zr-POMs in weakly alkaline solutions.

Interaction of Zr-POMs with H_2O_2 and Catalytic Oxidations in the Presence of Zr-POMs. Several ^{31}P NMR studies have implicated that many POMs are solvolytically not stable to H_2O_2 and, in fact, they often act as precursors of a true catalyst Venturello complex $\{PO_4[W(O)(O_2)_2]_4\}^{3-}$ and/or other low-nuclearity peroxotungstate species,[10,73−75] which are highly active as electrophilic O-transfer agents.[76,77] The stability of the $[PW_{11}O_{39}ZrOH]^{4-}$ structural unit toward an excess of H_2O_2 in MeCN was confirmed by several spectroscopic techniques. First, upon the addition of H_2O_2 to Zr-POMs ($[H_2O_2]/[Zr-POM] = 100$) and storage of the solution at 70 °C for at least 5 h, no products derived from the degradation of the Keggin structural unit were detected by ^{31}P NMR in the range of +7 to −11 ppm, where one could expect the appearance of lower nuclearity species.[73−75] Second, ^{183}W NMR confirmed the preservation of the C_s symmetry upon the addition of H_2O_2 to **1** (Figure 5e). Finally, Raman spectra of **1** in MeCN before and after the addition of H_2O_2 are identical (Figure 3a,b) after subtraction of the spectrum of H_2O_2 in MeCN (Figure 3c). The only new band, which appears after the addition of H_2O_2, is that located at 867 cm^{-1}, which belongs to free H_2O_2, as can be judged from Figure 3. No bands that could be attributed to a zirconium peroxo species were found.

We compared the catalytic behaviors of Zr-POMs prepared in this work in the oxidation of three representative organic substrates, TMP, CyH, and α-pinene, with aqueous H_2O_2. The oxidation of CyH with H_2O_2 in the presence of Zr-POMs was followed by ^{31}P NMR (Figure 6) and GC−MS. Upon the addition of a 20-fold excess of H_2O_2 to **1**, a broad signal at δ −12.3 ppm (Figure 6A) appeared. We mentioned above that the addition of water to **1** and **2** results in the upfield shift of the ^{31}P NMR resonance (Figure S5 in the SI), so the signal at δ −12.3 ppm is not due to the interaction of **1** with water. Moreover, this signal disappeared rapidly upon introduction of CyH; simultaneously, the resonance at δ −12.9 ppm arose (Figure 6B), and the formation of comparable amounts of 2-cyclohexen-1-one and *trans*-cyclohexane-1,2-diol along with traces of 2-cyclohexen-1-ol was detected by GC−MS. Note that CyH oxidation with H_2O_2 over heterogeneous Zr,Si catalysts also produced the diol (and/or its precursor, epoxide) along with the allylic oxidation products.[43,47]

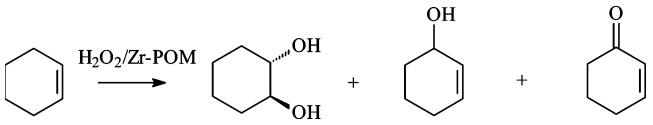

In the absence of CyH, the signal at δ −12.3 ppm also disappeared gradually, but the rate of its decay was signifi-

(73) Dengel, A. C.; Griffith, W. P.; Parkin, B. C. *J. Chem. Soc., Dalton Trans.* **1993**, 2683−2688.
(74) Salles, L.; Aubry, C.; Thouvenot, R.; Robert, F.; Doremieux-Morin, C.; Chottard, G.; Ledon, H.; Jeannin, Y.; Brégeault, J.-M. *Inorg. Chem.* **1994**, *33*, 871−878.
(75) Duncan, D. C.; Chambers, R. C.; Hecht, E.; Hill, C. L. *J. Am. Chem. Soc.* **1995**, *117*, 681−691.
(76) Venturello, C.; D'Aloisio, R.; Bart, J. C. R.; Ricci, M. *J. Mol. Catal.* **1985**, *32*, 107−110.
(77) Venturello, C.; D'Aloisio, R. *J. Org. Chem.* **1988**, *53*, 1553−1557.

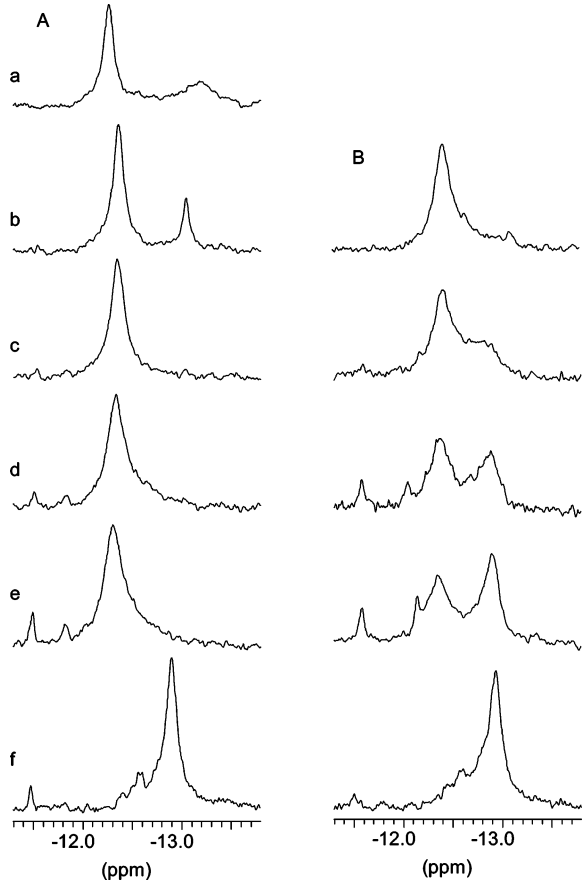

Figure 6. ^{31}P NMR spectra of **1** (0.01 M in MeCN, 20 °C) in the course of time: 0 (a), 1 (b), 35 (c), 102 (d), and 210 (e) min and 3 days (f) after the addition of 0.2 M H_2O_2 (A) and after the addition of 0.2 M H_2O_2 followed by the immediate addition of CyH (B).

cantly lower. After several days, the signal at −12.9 ppm became predominant both with and without CyH (Figure 6). All of these allowed us to assign the ^{31}P NMR resonance at δ −12.3 ppm to an unstable Zr-POM peroxo species, active in the oxidation of organic substrates. In the case of **2**, a similar behavior was monitored by ^{31}P NMR, but the disappearance of the peroxo species signal took a longer period of time. In turn, no changes in the ^{31}P NMR spectrum of **3** were detected upon the addition of H_2O_2 and no products of CyH oxidation were found. All of these facts collectively allowed us to suggest that the active peroxozirconium species might form upon substitution of the water ligand in the coordination sphere of the monomeric species $(n\text{-}Bu_4N)_{3+n}[PW_{11}O_{39}Zr(OH)_n(H_2O)_{3(2)-n}]$ by a peroxo (H_2O_2) ligand. The peroxo species signal broadening may be due to exchange between species containing different amounts of peroxo groups. Our first attempts to isolate this peroxozirconium species and to clarify its structure failed because of the fast dismutation of H_2O_2 in the presence of Zr-POMs. Note that significant H_2O_2 decomposition is also typical of heterogeneous Zr,Si catalysts.[48]

The results on the catalytic activity of **1**−**3** in H_2O_2-based oxidation of another representative alkene, α-pinene, are given in Table 3. As in the case of CyH, **3** is practically inactive in α-pinene oxidation. Hence, we may conclude that acid protons are crucial for the catalytic activity of Zr-POMs such as was found previously for Ti-POMs.[36−41] The oxidation of α-pinene affords the allylic oxidation products, verbenol and verbenone, along with campholenic aldehyde. The oxidation selectivity strongly depends on the alkene conversion; at high conversions, unidentified oligo/polymerization products formed because of prevailing overoxidation. The product of α-pinene rearrangement, camphene, was also found.

Table 3. Oxidation of α-Pinene with H_2O_2 in the Presence of **1**−**3**[a]

Zr-POM	α-pinene conversion,[b] %	TOF,[c] h^{-1}	verbenol yield,[d] %	verbenone yield,[d] %
1	40	14	21	18
2	25	8	35	40
3	7	0.8	nd	nd
e	5	nd	nd	nd

[a] Reaction conditions: α-pinene, 0.1 M; H_2O_2, 0.12 M; Zr-POM, 0.0025 M; MeCN, 30 °C, 1 h. [b] The main detectable products were verbenol, verbenone, campholenic aldehyde, and camphene. [c] TOF = (moles of substrate converted in the catalytic reaction − moles of substrate converted in the blank experiment)/(moles of Zr-POM × h). [d] GC yield based on α-pinene consumed. Similar amounts of campholenic aldehyde and camphene (rearangement product) were also found along with unidentified high-boiling products formed from overoxidation. [e] No catalyst was present.

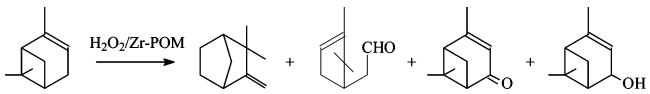

Recently, we found the same set and similar distribution of products in the presence of a heterogeneous Zr-single-site catalyst, Zr-MCF.[49] The similarity in the catalytic behavior of Zr-POMs and heterogeneous Zr catalysts supports our concept about using Zr-POMs as soluble probes for studying the mechanisms of heterogeneous Zr-catalyzed oxidations.

The catalytic activity of Zr-POMs in TMP oxidation with H_2O_2 decreased in the order Zr-HPA > **1** ∼ **2** > **3**. Figure 7A shows kinetic curves for TMP consumption demonstrating this order. Some activity of **3**, which was almost inert with alkenes, in this reaction may be due to the protic nature of the phenolic substrate. It is worth noting that the established order of the catalytic activity of Zr-POMs in H_2O_2-based oxidation of organic substrates correlates with the rates of H_2O_2 decomposition in the presence of Zr-POMs (Figure 7B).

The catalytic TMP oxidation in the presence of Zr-POMs yielded 2,3,5-trimethyl-*p*-benzoquinone (TMBQ) and 2,2′,3,3′,5,5′-hexamethyl-4,4′-biphenol (BP) as the main reaction products (Table 4).

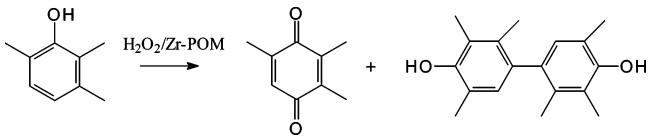

The same products were found recently in TMP oxidation by H_2O_2 in the presence of Ti-POMs.[39,40] The selectivity to TMBQ was maximal for **1** and attained 45% at 90% TMP conversion.

The products of the oxidation of TMP, CyH, and α-pinene that we found in the presence of Zr-POMs are consistent

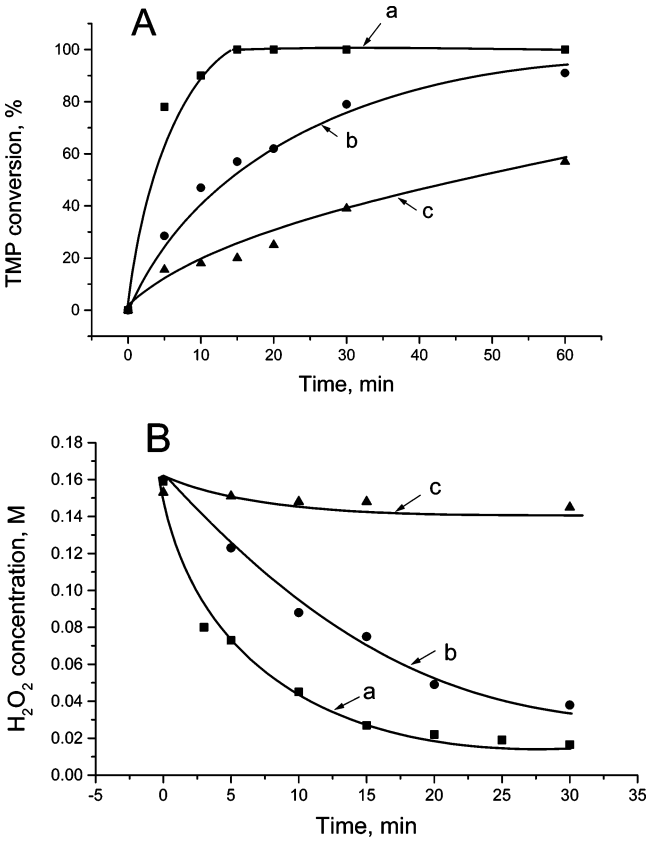

Figure 7. Oxidation of TMP (0.1 M) with H_2O_2 (0.35 M) at 80 °C (A) and H_2O_2 decomposition at 35 °C (B) in the presence of Zr-POMs ([Zr-HPA] = 0.005 M; [**1**] = [**3**] = 0.0025 M) in MeCN: Zr-HPA (a), **1** (b), and **3** (c).

Table 4. TMP Oxidation with H_2O_2 in the Presence of Zr-POMs[a]

Zr-POM	TMP conversion, %	TOF,[b] h^{-1}	TMBQ yield,[c] %
1	90	60	45
3	37	32	30

[a] Reaction conditions: TMP, 0.1 M, H_2O_2, 0.35 M, Zr-POM, 0.0025 M, MeCN, 1 mL, 80 °C, 1 h. [b] TOF = (moles of TMP consumed)/(moles of Zr × h); determined from the initial rates of TMP consumption. [c] GC yield based on TMP consumed. The main byproduct was BP; small amounts of C−O-coupling products were also detected by GC−MS.

with one-electron oxidation mechanisms.[78] This fact allows exclusion of peroxotungstate species as reactive intermediates because such species are expected to afford products typical of a two-electron electrophilic O-transfer mechanism. Specifically, high selectivity to epoxides/diols would be expected for alkene oxidation by peroxotungstate complexes. The reaction rate and products are similar in an inert atmosphere (Ar) and in air. Additionally, the reaction is not retarded by small amounts of the radical-chain scavenger, 2,6-di-*tert*-butyl-4-methylphenol (ionol). These two facts argue in favor of a non-radical-chain mechanism or suggest short radical chains. In sharp contrast to Ti-POMs, no change of the reaction mechanism occurred with an increase in the proton amount in Zr-POMs. While Ti-substituted heteropolyacid $H_5PW_{11}TiO_{40}$ and its acid salts catalyze heterolytic CyH oxidation, producing *trans*-cyclohexane-1,2-diol as the major reaction product,[41] Zr-HPA yields mainly the allylic oxidation product, 2-cyclohexen-1-one, along with minor amounts of 2-cyclohexen-1-ol, diol, and cyclohexanol, which arises most likely via Zr-HPA-catalyzed hydration of CyH.

Conclusions. Three forms differing in their protonation state, $(n\text{-}Bu_4N)_7H[\{PW_{11}O_{39}Zr(\mu\text{-}OH)\}_2]$ (**1**), $(n\text{-}Bu_4N)_8[\{PW_{11}O_{39}Zr(\mu\text{-}OH)\}_2]$ (**2**), and $(n\text{-}Bu_4N)_9[\{PW_{11}O_{39}Zr\}_2(\mu\text{-}OH)(\mu\text{-}O)]$ (**3**), of the previously unknown Zr^{IV}-monosubstituted Keggin-type POM have been prepared and comprehensively characterized. Using a combination of elemental analyses, potentiometric titration, X-ray single-crystal structure analysis, IR, Raman, and ^{31}P and ^{183}W NMR, it has been revealed that in **2** two Keggin structural units $[PW_{11}O_{39}Zr]^{3-}$ are connected through two hydroxo bridges Zr−(OH)−Zr with Zr^{IV} in 7-fold coordination; the addition and removal of one proton lead to forms **1** and **3**, respectively. In agreement with the experimental characterization of **1**−**3**, DFT calculations showed that protonation at the Zr−O−Zr bridging O atom leads to the most stable complex because of the intrinsic basicity of this site. Moreover, calculations indicate that for Zr-monosubstituted dimers the doubly bridged hydroxo species are thermodynamically more stable than the singly bridged oxo ones, which contrasts with that observed for the Nb[71] and Ti[36,40] analogues. A comparison of the bond strengths reveals that the Zr−O bond is only slightly stronger than the Zr−OH bond; however, this energy difference can be largely compensated for by the protonation energy. Two, one, and no protons in **1**−**3**, respectively, possess acid properties. The acid protons assist the interaction of the dimeric Zr-POM with H_2O in MeCN to produce monomeric species, most likely $(n\text{-}Bu_4N)_{3+n}[PW_{11}O_{39}Zr(OH)_n(H_2O)_{3-n}]$ (n = 0 and 1), as well as the interaction with H_2O_2, leading to the formation of peroxozirconium species capable of oxidizing organic substrates via homolytic oxidation mechanisms. The catalytic behavior of Zr-POMs in H_2O_2-based oxidations is similar to that of heterogeneous Zr-single-site catalysts.

Acknowledgment. We thank V. Utkin and Dr. V. Rogov for GC−MS analyses, Yu. Chesalov for IR measurements, Drs. E. Chubarova and M. Timofeeva for preliminary results on the catalytic activity of Zr-POMs, and Dr. I. Baydina for preliminary X-ray data. We are also grateful to Profs. V. Fedin, M. Sokolov, and M. Fedotov for fruitful discussions. The Russian Foundation for Basic Research (Grant N 04-03-32113) partially funded the research. This work was also supported by the Spanish MECD (Grant BQU2002-04110-C02-01) and the CIRIT of the Autonomous Government of Catalonia (Grant SGR01-00315). N.S.A. thanks the Spanish MECD for a predoctotal grant.

Supporting Information Available: Crystallographic data for **2** in CIF format, packing diagrams of **2**, potentiometric titration curves of **1** and **2**, IR and Raman spectra of solid **1**−**3**, ^{31}P NMR spectra of **1** in MeCN as a function of added H_2O, polyhedral and ball-and-stick views of **2** and **2b**, and bond lengths, atomic coordinates, and equivalent isotropic and anisotropic displacement parameters for compound **2**. This material is available free of charge via the Internet at http://pubs.acs.org.

IC0608142

(78) Sheldon, R. A.; Kochi, J. K. *Metal-Catalyzed Oxidations of Organic Compounds*; Academic Press: New York, 1981.